geoconvention
Virtual Event
September 21-23
2020
CSPG • CSEG • CWLS • GAC • MAC • IAH

Clay-Dependent Rock Physics Approach to Pore Pressure Prediction – An Example from East Coast Canada

Joel K Loeffler[1], Lev Vernik[2]
[1]Ikon Science Canada, [2]Ikon Science Americas

Summary

Industry standard pore pressure prediction techniques (Equivalent Depth and Eaton Ratio methods) rely on a host of assumptions to be met before an accurate pressure prediction can be generated. Two factors that are often not accounted for are relative changes in clay content (v_{clay}) and total organic carbon (TOC) vertically across geologic formations as well as laterally on basin scales.

The case study presented here illustrates a workflow designed to account for the lithological variability associated with clay content and its effect on wireline response through a series of rock physics models (RPMs). Accounting for changes in v_{clay} within a pore pressure workflow will lead to a more robust pressure model.

Introduction

Traditional pore pressure prediction techniques rely on various assumptions for their application. In general, it is assumed that shales are at their maximum burial depth, have not been subjected to elevated temperatures (>80°-100°C) or undergone significant clay diagenesis, and a clear relationship between porosity and effective stress exists. Typically, it is assumed the primary pore pressure generating mechanism is disequilibrium compaction; a process through which the inability of fine-grained/clay-rich sediments to dewater in response to increasing stresses leads to the shale retaining higher porosity relative to a normally compacted rock at the same depth. The higher porosity leads to higher pore pressure (lower effective stress) as the fluid phase must support more of the overburden load. The porosity is linked to elevated pore pressures via porosity-effective stress models such as the Equivalent Depth Method (Foster & Whalen, 1966), Eaton Ratio Method (Eaton, 1975), and the Vp-Effective Stress Method (Bowers, 1994); all of which attempt to use the relationship between vertical stress (S_v) and vertical effective stress (σ'_v) to back out pore pressure (P_P) following the Terzaghi principle (Equation 1; Terzaghi, 1943). Pore pressure prediction is usually derived as a function of the vertical stress but any process that results in an increase in the mean stress can help to generate (or maintain) pore pressure.

$$P_P = S_v - \sigma'_v \qquad (1)$$

Crucially, each of these methods presumes deviations in the wireline log response (Vp, Vs, Rho, Neutron, and Resistivity) are directly a result of changes in porosity, and fails to recognize other contributing factors that can affect wireline logs. For example, mineralogy, fluid saturation, salinity, pore shape, and crack density can all influence log response, and therefore pressure predictions.

Most commonly, the sonic (Vp) log is used for pressure prediction as it is the compressional velocity that is most easily derived in the seismic domain. In this case, fluctuations in v_{clay} and

TOC are the most likely to result in large variations in measured velocities; both vertically and laterally across a basin. Increases in v_{clay} and TOC both act to reduce measured velocities (and density), mimicking the effect increased pore pressure has on elastic logs. Therefore, in formations where v_{clay} and TOC are variable, the magnitude of anticipated pore pressure may show large deviations as natural variations in lithology are encountered well-to-well. While the focus of this exercise is to illustrate how to account for variable clay-content, Green & Vernik (2020; *In Submission*) provide an example on how correcting elastic logs for TOC can aid in the pressure prediction workflow. As an accurate pore pressure prediction is a crucial input into well design, accounting for these variations can lead to more efficient drilling programs as optimizations to mud plans, casing design, and reductions in NPT are all possible.

Method

As pressure prediction workflows generally focus on linking shale porosity (by proxy of wireline logs) to vertical effective stress, one of the first steps in the workflow is typically to produce an estimation of the shale-volume fraction (V_{shale}). Various petrophysical methods exist to estimate V_{shale}, though in an effort to simplify the workflow, V_{shale} is often calculated using the gamma-ray (GR) log. The resulting V_{shale} log is used to create cut-offs and indicate over which zones or intervals a pore pressure prediction workflow will be completed. By generating a linear interpolation of GR, the gamma-ray index (*G*) is calculated as a function of the normalized gamma-ray (GR_n), along with baselines for a clean sand (GR_{min}) and the shale gamma-ray response (GR_{max}). The shale fraction can be taken as V_{shale} = *G* and scaled between 0 and 1.

While this approximation of V_{shale} is quick, and helpful in distinguishing shales from non-shales, it does little to quantify the variations in clay content (v_{clay}) that may be occurring within shales. As none of the traditional porosity-effective stress models for predicting pore pressure include a shale-volume fraction input, it is little more than an afterthought once non-shales have been filtered out. Further, it is the clay content (mineralogical variable) rather than the shale-volume fraction (lithological variable) that will have an influence on the magnitude of the elastic log response (velocity and/or density). It is this fundamental distinction that should lead to a more accurate pressure prediction.

Like V_{shale}, v_{clay} can be reliably estimated via wireline logs, namely neutron and bulk-density (ρ_b) or more specifically through a crossplot of neutron/density porosity. Initially, apparent density porosity (ϕ_D) is calculated, as a function of ρ_b (Equation 2), where ρ_{ma} and ρ_{fa} are the apparent matrix and fluid densities, respectively. The neutron porosity (ϕ_N) can then be related back to the density porosity via Equation 3.

$$\phi_D = (\rho_{ma} - \rho_b)/(\rho_{ma} - \rho_{fa}) \quad (2)$$

$$\phi_N = b\phi_D + a \quad (3)$$

In (3), a is the intercept (neutron/density porosity crossplot), which represents the share of the hydrogen index attributed to the clay component, in terms of neutron porosity. The slope (b) is taken to be 0.875, which is widely applicable in siliciclastics with porosities less than 40% (Vernik, 2016). When plotting ϕ_D against ϕ_N, two parallel trend lines corresponding to v_{clay}= 0 and v_{clay}= 1 can be positioned tangential to 'clean sands' and 'clean shales' such that the intercepts (a_{sd} and a_{sh} respectively) can be used to generate values of v_{clay} following Equation 4.

$$v_{clay} = \frac{(\phi_N - b\phi_D - a_{sd})}{a_{sh} - a_{sd}} \tag{4}$$

Preferably, core analysis has been undertaken and a reliable set of XRD measurements are available to calibrate the calculated v_{clay}, though in the absence of lab data the estimation can be sensibly constrained. However, it is important to recognize the v_{clay} estimation is integral to this workflow, and as such great care should be taken in its estimation.

With a reliable v_{clay} estimation, the bedding-normal elastic stiffness can be calculated for both the bulk rock, as well as the matrix (C_{33} and C_{33m}, respectively). Vernik and Kachanov (2010) showed that a heuristic clay-based model relating bedding-normal velocity ($Vp(0°)$) to shales with 40-45% porosity is compatible with the compaction behavior of shales as effective stress increases. The model assumes the shale has a bimodal composition: (i) the aligned/laminated clay platelets, and (ii) the non-clay component. Thus, the bedding-normal matrix stiffness can be computed using Reuss averaging (Vernik, 2016):

$$Vp(0°) = \sqrt{\frac{C_{33m}(1-\phi)^{k^*}}{\rho_m(1-\phi)+\rho_f\phi}} \tag{5}$$

$$C_{33m} = \{v_{clay}/C_{33clay} + (1 - v_{clay})/M_{quartz}\}^{-1}$$

where k^* is an empirical clay-dependent exponent ($k^* = 5.3 - 1.3v_{clay}$), ϕ is total porosity, and ρ_m and ρ_f are the matrix and fluid densities. In shales with porosities less than 40%, empirical models can be used in their place:

$$\begin{aligned} Vp(0°) &= Vp_m(1-\phi)^k \\ Vp_m &= 5.69km/s - 3.56v_{clay} + 1.42{v_{clay}}^2 \\ k &= 2.302 - 0.646v_{clay} \end{aligned} \tag{6}$$

When plotted against Vp-Total Porosity (Figure 1), the resulting clay-content estimation from Equation 6 shows a good fit to the rock physics model. Unfortunately, core data was not available for this well, so the model could not be calibrated against absolute values of clay content. Globally, clay content in shales typically ranges between 30-90%, while in the Gulf of Mexico 40-65% is common. Here, a value of ~60% appears to approximate a majority of the interval and is consistent with average shales worldwide (Vernik, 2016). By adjusting Equation 6, and incorporating Rubey and Hubbert's (1959) exponential relationship for porosity and effective stress, the bedding-normal sonic velocity can be calculated for a given vertical effective stress:

$$Vp(0°) = V_{Pm}[1 - \phi_o exp(-\sigma_v'/C_m)]^k \tag{7}$$

where C_m is the inelastic compaction modulus and typically ranges between 24 and 31 MPa (Vernik, 2011) for shales experiencing loading, as opposed to unloading mechanisms (Bowers, 1994). As with Equation 6, this model only applies to shales with porosities ≤40-45%, and thus should not be used in close proximity to mudline where mudrocks are still undergoing rapid compaction. Substituting hydrostatic pressure for pore pressure in Equation 1, results in the normal vertical effective stress, which can be plugged into Equation 7 in place of σ_v'. In this case, Equation 7 becomes a normal compaction trend (NCT). The advantage of this approach is the resultant NCT varies in accordance with changes in clay-content, unlike typical NCTs that rely on a single exponential fit. A common workaround employed in traditional pressure workflows when the elastic behavior of shales is seen to materially change within a well is to invoke an additional NCT, and often with good reason such as a change in provenance, clay type, or unconformities. However, this approach is not without its limitations, namely the inability to account for variation *within* a contiguous shale, as well as relying on the interpreter to decide when *some* variation becomes *too much* variation for a given NCT.

As a final step in the clay-based pressure prediction workflow, the vertical effective stress is calculated from Equation 7, and inputted into Equation 1 to calculate the pore pressure.

$$\sigma_v{}' = C_m \ln\left[\phi_0/\left(1-(Vp/Vp_m)^{\frac{1}{k}}\right)\right] \tag{8}$$

Results

The workflow described above has been applied to an East Coast Canada well, and the results are shown in Figure 2. Both Equivalent Depth (Vp) and Eaton Ratio (Vp/Resistivity) methods were calibrated to neighboring wells. Pressure measurements (green diamonds) show the sands to be laterally drained and near-normally pressured, as is common for this area (O'Connor et al., 2012). All four methods indicate the shale interval, coloured purple (~x900 to x250m), to be overpressured (~14ppg EMW) and drilled underbalanced. However in the upper 100m of the interval (dark red shaded region), there is a change in the elastic logs, manifested by an increase in Vp & Density, as well as a shift in the neutron log; these changes correspond to an increase in the siltstone fraction as seen in drill cuttings (track 2), and can be observed in the surrounding wells. The traditional methods, using a single NCT, associate this increase in Vp to a decrease in shale porosity, and therefore a marked decrease in pore pressure (~10ppg EMW). The clay-based pressure prediction accounts for the clay-content based on the changes in neutron-density, and produces a prediction (13.5ppg EMW) consistent with the lower portion of the shale interval. Both sets of interpretations imply a shoulder effect to be present at the top of the shale, as would be expected as the overlying sands (shaded light blue) are believed to be normally pressured. Although this example covers a limited depth range, the learnings here can be used to inform casing and mudweight design for subsequent wells.

References

Bowers, G.L. 1994. Pore pressure estimation from velocity data: accounting for overpressure mechanisms besides under-compaction. IADC/SPE Drilling Conference, 27488.

Eaton, B.A. 1975. The equation for geopressure prediction from well logs. Society of Petroleum Engineers 5544.

Foster, J. B. and Whalen, H. E., 1966, Estimation of Formation Pressures From Electrical Surveys-Offshore Louisiana, Journal of Petroleum Technology, 18 (2), pp. 165–171.

O'Connor, S., Green, S., Swarbrick, R., and Lahann, R., 2012, Lateral drainage in the Jeanne d'Arc and Flemish Pass Basins, East Canada [abstract], In: Geoconvention May14-18, 2012, Calgary, Alberta, Canada.

Rubey, W. W., and M. K. Hubbert, 1959, Role of fluid pressure in mechanics of overthrust faulting II: Overthrust belt in geosynclinals area of western Wyoming in light of fluid-pressure hypothesis: Geological Society of America, Bulletin 70, no. 2, 167-206.

Terzaghi, K., 1943, Theoretical Soil Mechanics. New York: John Wiley and Sons.

Vernik, L., 2011, Unified model for continuous pore pressure prediction in shale: 45th US Rock Mechanics/Geomechanics Symposium, American Rock Mechanics Association, conference paper ARMA-11-444.

Vernik, L., 2016, Seismic petrophysics in quantitative interpretation. Society of Exploration Geophysicists.

Vernik, L., and M. Kachanov, 2010, Modeling elastic properties of siliciclastic rocks: Geophysics, 75, no. 6, E171-E182.

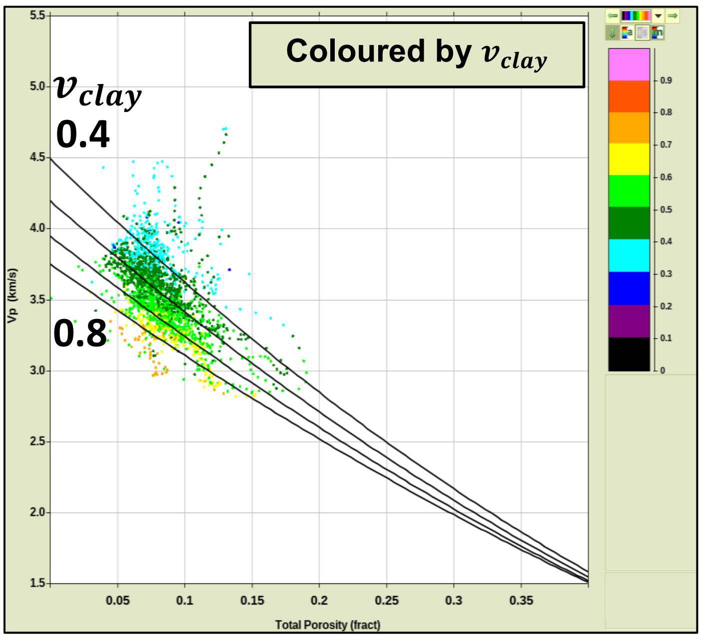

Figure 1 (left): Vp-Total Porosity crossplot, coloured by v_{clay}. Solid lines indicate Vp-total porosity relationships as given by the RPMs in equation 6. A good fit to the RPM shows the v_{clay} calibration from neutron-density to be applicable to this shale.

Figure 2 (below): Log data from an East Coast Canada well. In the Pressure-Depth plot to the right, the clay-based pressure curve (red) is plotted against traditional methods. Dotted lines indicate average pressure gradients from the drill floor in equivalent mudweight (EMW) from 8-20ppg.